
MITIGATING LEARNING COMPLEXITY IN PHYSICS AND EQUALITY CONSTRAINED ARTIFICIAL NEURAL NETWORKS

A PREPRINT

 Shamsulhaq Basir* and  Inanc Senocak†

*Department of Mechanical Engineering and Materials Science, University of Pittsburgh,
3700 O'Hara St., Pittsburgh, PA 15261, USA*

ABSTRACT

Neural networks can be used to learn the solution of partial differential equations (PDEs) on arbitrary domains without requiring a computational mesh. However, this learning process can become complex and challenging for a certain class of PDE problems. Here, we show that perturbations present in the output of a neural network model during early stages of training lead to higher levels of noise in a structured loss function composed of high-order differential operators. These errors corrupt the back-propagated gradients and impede convergence. We demonstrate the learning complexity issue with tractable problems and mitigate it by introducing auxiliary flux parameters in second-order PDEs to obtain a system of first-order differential equations. We formulate a non-linear constrained optimization problem aimed at minimizing the sum-of-squared errors of the residual form of a first-order PDE subject to the boundary conditions as well as the auxiliary flux equation. We recast the constrained optimization problem as an unconstrained dual problem using the augmented Lagrangian method. We apply our approach to learn the solution of various second-order PDE problems including heat transfer in a composite medium, singularly perturbed reaction-diffusion, and convection-dominated convection-diffusion equation and demonstrate orders of magnitude improvement over existing approaches.

Keywords Constrained optimization · Augmented Lagrangian method · machine learning · meshless method

1 Introduction

Partial differential equations (PDEs) play a vital role in our comprehension of a wide range of physical phenomena, including sound propagation, heat and mass transfer, fluid flow, and elasticity to name a few. Most of the modern problems involving PDEs are usually solved via numerical methods, owing to the lack of closed analytical solutions. The most common and powerful numerical methods for solving PDEs are finite volume, finite difference, finite element, and spectral element methods. Although these methods are highly efficient in solving forward problems, they do not readily extend to data-driven modeling and inverse problems. Furthermore, quality mesh generation is an essential part of conventional numerical methods, which can be tedious and time consuming for problems involving complex geometry. To this end, neural networks as universal approximators [1] can be viewed as an alternative meshless approach to solve PDEs in either a strong or weak form by randomly distributing points within the solution domain.

Dissanayake and Phan-Thien [2] and van Milligen et al. [3] are credited with introducing neural networks as an alternative solution technique for PDEs. Their pioneering approach with neural networks have been applied to learn the solution of different types of PDEs with satisfactory results [4, 5, 6, 7]. Different from those previous works, Lagaris et al. [8] proposed a neural network-based method for the solution of differential equations on orthogonal box domains. Their approach relies on constructing custom trial functions that satisfy boundary conditions by construction. However, their is limited to simple domains for which it is trivial to create trial functions. In addition, creating trial

*shb105@pitt.edu (Shamsulhaq Basir)

†corresponding author: senocak@pitt.edu (Inanc Senocak)

functions impose prior bias toward a certain class of functions that might not be optimal for the problem at hand. Most recently, several researchers have taken a similar approach to apply neural networks for the solution of differential equations either in the weak or strong form [9, 10, 11]. E and Yu [9] proposed the Deep Ritz method for the solution of PDEs. However, their method is only applicable to problems that can be formulated as energy minimization problems. Sirignano and Spiliopoulos [11] proposed Deep Galerkin method (DGM) for the solution of high-dimensional PDEs. Similar to the early works in [2, 3, 6], Raissi et al. [10] proposed physics-informed neural networks (PINNs) using a modern deep-learning framework TensorFlow [12]. The interest to use neural networks to learn the solution of PDEs continues to grow at a fast pace with applications in various domains [13, 14, 15, 16, 17, 18, 19, 20, 21, 22]. In the present work, we refer to the technical approach pursued in [2, 3, 4, 6, 7, 10] as PINNs because the core formulation in these works are essentially the same.

A common technique pursued in PINNs is to minimize a weighted sum of several objective functions that are balanced with multiplicative weighting coefficients or hyperparameters. These hyperparameters are not known *a priori*. Many researchers have found that predictions from neural network models are highly dependent on these hyperparameters and *a priori* determination of them have been a research topic [23, 24, 25, 26, 27, 28, 29]. Wang et al. [25] demonstrated that PINNs do not produce consistent and physically feasible solutions when applied to various kinds of PDEs. Wang et al. proposed an empirical algorithm that improves over the conventional PINNs, but even their method has several limitations as we have discussed in our prior work [28]. van der Meer et al. [23] proposed a heuristic method to determine these hyperparameters by considering an affine combination of a physics-informed bi-objective loss function. However, their approach also has issues. First, it is not advisable to sum up objective functions with different scales to form a mono-objective optimization equation [30], because the objective function representing the residual on a given PDE and the one representing the mismatch on boundary conditions do not often share the same scale and, therefore, the learned hyperparameters no longer represent the relative importance of the objective functions. Second, for non-convex Pareto fronts, some optimal set of solutions cannot be found with any combination of the weighting factors [30]. In a different work [27], we visualized the loss landscapes of a trained data-driven neural network model and its physics-informed counterpart and demonstrated that incomparable scales between loss terms in a composite objective function impede the convergence of neural network models.

Recently, we proposed physics and equality constrained artificial neural networks (PECANNs) to learn the solution of forward and inverse problems [28]. Our PECANN framework is noise-aware and adept at multi-fidelity data fusion. The backbone of the PECANN framework is a constrained optimization formulation that is recast as an unconstrained optimization problem using the augmented Lagrangian method [31, 32]. The PECANN framework balances each term in the objective function in a principled fashion and enable the user to specify the degree of noise in observed data.

It is worth noting that in the PINN approach and as well as in the PECANN approach, L^2 norm is used in training the neural network. However, L^2 norm increases the learning complexity of the original problem [33], which is further elevated for PDE solutions that are ill-conditioned. Because the predictions of the network are often noisy or incorrect during the early stages of training, noise in the back-propagated gradients can be amplified and impede the convergence of PDE problems with ill-conditioned solutions.

The learning complexity can be mitigated by reducing the order of the differential operators. For instance, E and Yu [9] uses a variational formulation to reduce the order of a differential operator via integration by parts. However, their approach can be applied only to problems that can be formulated as an energy minimization problem. In addition, boundary conditions are soft-constrained in their approach by a penalty parameter that are not known *a priori*. Cai et al. [33] proposed a method that adopts least-squares functionals to train a deep neural network to learn the solution of one-dimensional elliptic PDEs. The least-squares functionals are based on the so-called first-order system least-squares (FOSLS). Through this approach, the authors are able to reduce the order of a given elliptic PDE by introducing an auxiliary flux parameter. Their method learns the primary variable and the auxiliary flux variable by a composite neural network with two branches. Since Sobolov norms (i.e. $\|\cdot\|_{1/2}$ or $\|\cdot\|_{-1/2}$) are computationally infeasible, the authors approximated them with weighted L^2 norms. Boundary conditions on the PDE are enforced as penalty regularizers with hyperparameters that are known in *a priori*. Differential operators are approximated using a finite difference scheme on a fixed mesh. However, requiring a computational mesh chips away the appeal of using neural networks as a meshless method. Also, finite difference approximation of derivatives requires multiple forward passes through the computational graph amplifying the inherent discretization errors, particularly for problems with multiple inputs. Whereas with automatic differentiation, which computes the derivatives in a single backward pass, derivatives can be calculated at machine precision [34].

In the present work, we demonstrate how structured objective functions that contains differential operators amplify noise in the learning process, which in turn corrupt the back propagated gradients. Consequently, the convergence of the learning process is impeded. This issue is amplified for PDE solutions that are inherently ill-conditioned. We quantify and demonstrate this ill-conditioning by calculating the relative condition number. We then propose a meshless

neural network-based solver for second-order PDEs that may not have any underlying energy minimization principles. We achieve this by introducing auxiliary flux parameters to reduce a second-order PDE to a first order system, which can also be viewed as preconditioning a given PDE and mitigating its learning complexity with neural networks. We formulate a constrained optimization problem aimed at minimizing the sum-of-squared errors of the residual form of the preconditioned differential equation subject to its boundary condition and the auxiliary flux equations. Unlike the composite neural-network approach adopted in [33], where numerical quadrature is used to compute the first-order system, our proposed method uses a single neural network architecture and employ automatic differentiation (AD) [34]. We use our PECANN framework [28] to enforce the boundary conditions on the first-order system without the need to manually balance the loss terms in the objective function through hyperparameters. We should note that optimal choice of hyperparameters are problem specific and does not transfer across different problems or even a different training setting for the same problem. Tuning these hyperparameters by trial and error is impractical if no information about the solution is available. Thanks to the augmented Lagrangian method adopted in the PECANN framework, there is no need to manually tune these hyperparameters. For appraisal of all the relevant information in this work, we open sourced our codes at https://github.com/shamsbasir/mitigating_learning_complexity_PECANNs.

1.1 Back-propagated Gradients in the Presence of Noise

In this section, we demonstrate how a differential operator amplifies noise in the predicted solution and, hence, corrupt the back-propagated gradients which may impede convergence. We use a simple one-dimensional Poisson's equation to explain this issue as follows:

$$\frac{d^2u(x)}{dx^2} = f(x), \forall x \in \Omega = [0, 1], \quad (1)$$

$$u(x) = g(x), \in \partial\Omega, \quad (2)$$

where Ω is the domain with its boundary $\partial\Omega$, $f(x)$ and $g(x)$ are source function and boundary function respectively. We manufacture a simple solution as $u(x) = \sin(5\pi x)$ for the above differential equation. $g(x)$ and $f(x)$ can be calculated exactly using the manufactured solution. The objective function using the PECANN framework[28] can be written as follows:

$$\mathcal{L}(\theta) = \sum_{i=1}^{N_\Omega} \left\| \frac{d^2\hat{u}(x^{(i)})}{dx^2} - f(x^{(i)}) \right\|_2^2 + \sum_{i=1}^{N_{\partial\Omega}} \lambda^{(i)} \phi(\hat{u}(x^{(i)}) - g(x^{(i)})) + \frac{\mu}{2} \pi, \quad (3)$$

$$\pi = \sum_{i=1}^{N_{\partial\Omega}} \left\| \phi(\hat{u}(x^{(i)}) - g(x^{(i)})) \right\|_2^2, \quad (4)$$

where \hat{u} is the prediction of our neural network model, $\lambda \in \mathbf{R}^2$ is a vector of Lagrange multipliers, μ is a positive penalty parameter and ϕ is a quadratic distance function, which we discuss further in section 2.1. For this one dimensional problem, the number of boundary points $N_{\partial\Omega}$ is 2. We note that the objective function given in Eq. (3) has a second order differential operator.

We carry out a numerical experiment to demonstrate the impact of a second-order differential operator on corrupting the back-propagated gradients in the presence of perturbations in the predicted solution during training. In our example, we use a feed-forward neural network with two hidden layers and 20 neurons per layer. We use a Sobol sequence with $N_\Omega = 256$ residual points uniformly in the domain as well as two boundary conditions only once before training.

First, we train our network for 1000 epochs and predict the solution from our neural network model $u(x; \theta)$ for comparison purposes. We also record the parameters of the network (i.e., θ) and their gradients (i.e., $\nabla \mathcal{L}_\theta$). Next, we perturb our parameters (i.e., θ) to obtain a new set of parameters (i.e., $\tilde{\theta}$). Perturbations are generated using two random Gaussian vectors with appropriate scaling as proposed in [35]. We then make a prediction from our neural network model $u(x; \tilde{\theta})$ at the perturbed state. We then obtain the back-propagated gradients (i.e., $\nabla \mathcal{L}_{\tilde{\theta}}$) at the perturbed state.

From Figs. 1(a) and (b) we observe that the distribution of the parameters of our network at the end of training and after the addition of perturbations are fairly similar, which indicates acceptable levels of noise or perturbations.

Next, we investigate the impact of the perturbations on the predictions obtained from our neural network model. In Fig. 2(a), we observe that our model has produced an acceptably accurate prediction of the solution after training without any perturbations. However, after the addition of perturbations, the prediction of our model $u(x; \tilde{\theta})$ distinctly deviates from the exact solution as seen in Fig. 2(a). The error resulting from this deviation is plotted in Fig. 2(b), which quantifies the absolute point-wise difference between the prediction of our model before and after the injection of noise in the parameters θ of our neural network.

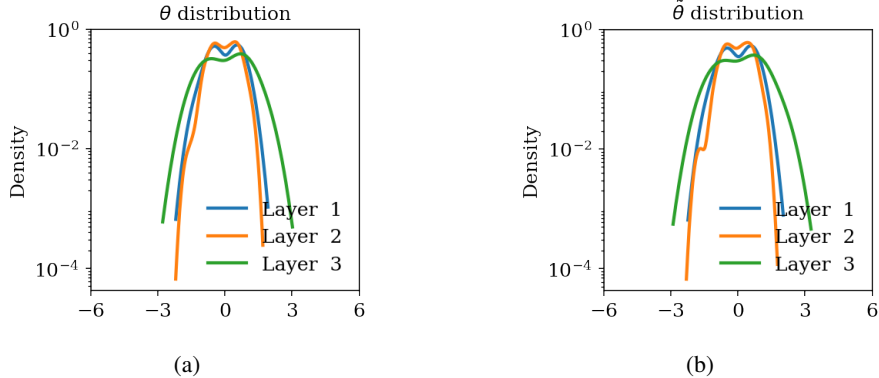


Figure 1: Distribution of the parameters of our neural network model at different states: (a) at the end of training for 1000 epochs, (b) after injection of perturbations

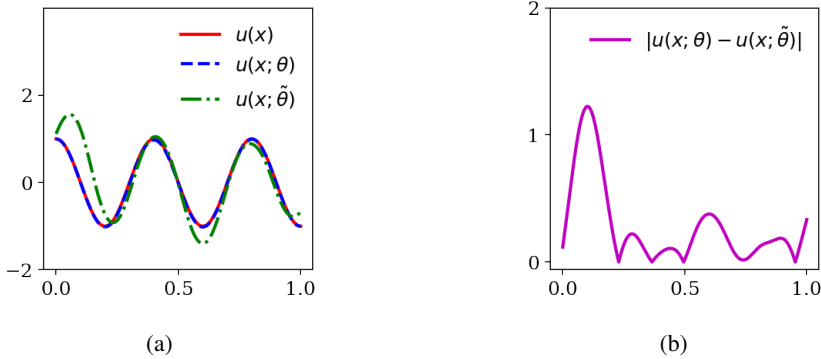


Figure 2: (a) exact solution $u(x)$, predicted solution $u(x; \theta)$ in dashed blue obtained from our neural network model after training for 1000 epochs, predicted solution $u(x; \tilde{\theta})$ in dashed green obtained from our neural network model at the perturbed state, (b) absolute point-wise difference between $u(x; \theta)$ and $u(x; \tilde{\theta})$,

Furthermore, in Fig. 3(a), we observe deviation of the first-order derivative of the prediction of our model before and after noise injection. This deviation as can be seen from Fig. 3(b) is one order of magnitude higher than the one in Fig. 2(b), which clearly shows that a first-order differential operator on a noisy output produces a much higher level of noise in the first order derivative. Therefore, we deduce that noisy outputs result in even noisier derivatives, which in turn amplifies the noise in the physics loss term.

From Figs. 4(a) and (b), we observe that deviations become severe between the second-order derivative of the predictions obtained from our model before and after the noise injection. This illustration reinforces our earlier conclusion that noisy outputs amplify noise in the derivatives such that the higher the order of the derivative operators, the larger the level of noise.

Finally, from Fig. 5(a), we observe that the gradients of the parameters of the neural network before the noise injection are concentrated near zero, which shows that the optimizer has approached a local minimum. However, after the noise injection, we observe that the gradients of the parameters of the neural network have increased by an order of magnitude, which demonstrates the impact of physics loss on amplifying the perturbations and, consequently, corrupting the gradients. In other words, corrupting the gradients may result in impeding or preventing the optimizer from convergence since it will affect the parameters which in turn perturb the solution of the model. Therefore, we conclude that learning solutions arising from low-order derivative operators are favorably easier to learn than learning solutions arising from high-order derivative operators.

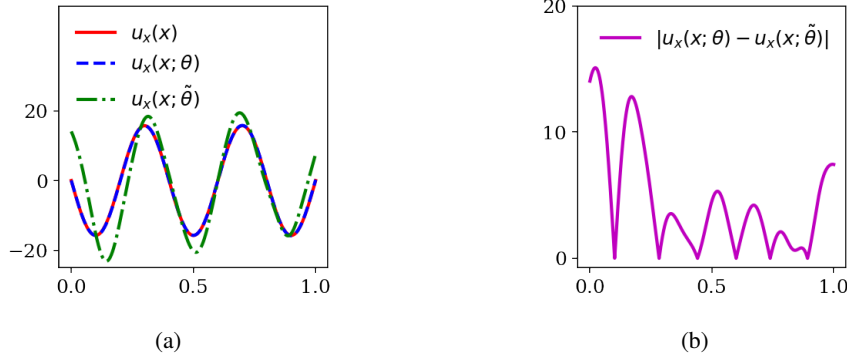


Figure 3: First-order derivative of the prediction obtained from our neural network model at different states: (a) comparison of the exact first derivative $u_x(x)$, predicted first derivative $u_x(x; \theta)$ obtained from the neural network model after training for 1000 epochs, and predicted first derivative $u_x(x; \tilde{\theta})$ obtained from the neural network model at the perturbed state, (b) absolute point-wise difference between $u_x(x; \theta)$ and $u_x(x; \tilde{\theta})$

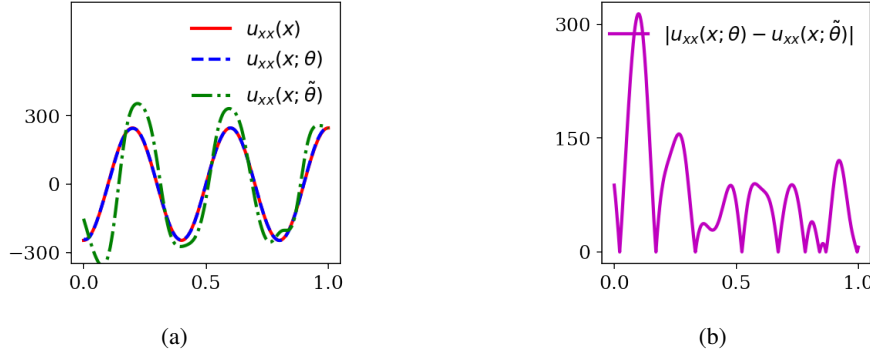


Figure 4: Second-order derivative of the prediction obtained from the neural network model at different states: (a) comparison of the exact second derivative $u_{xx}(x)$, predicted second derivative $u_{xx}(x; \theta)$ obtained from the neural network model after training for 1000 epochs, predicted second derivative $u_{xx}(x; \tilde{\theta})$ obtained from the neural network model at the perturbed state, (b) absolute point-wise difference between $u_{xx}(x; \theta)$ and $u_{xx}(x; \tilde{\theta})$

Next, we mathematically quantify the challenge of learning the solution of a well-posed PDE with neural networks. Consider the following functional relation

$$F(x, u) = 0, \quad (5)$$

where x (input) is the set of data on which the solution u (output) depends and F is the functional relation between x and u . Following the presentation in Quarteroni et al. [36], a relative condition number can be defined as follows

Definition 1 (Relative condition number)

$$\kappa(x) = \frac{\|\delta u\|/\|u\|}{\|\delta x\|/\|x\|}, \quad \delta x \neq 0, \quad (6)$$

where κ is the condition number, δx is a small perturbation in the data, and δu is the corresponding perturbation in the solution. If Eq. (5) admits a unique solution, then a mapping function G between the set of data x and the solution u necessarily exists

$$u = G(x), \quad F(G(x), x) = 0. \quad (7)$$

Hence, we can write the relative condition number as given in Eq. (6) in the following form

$$\kappa(x) = \|G'(x)\| \frac{\|x\|}{\|G(x)\|}, \quad (8)$$

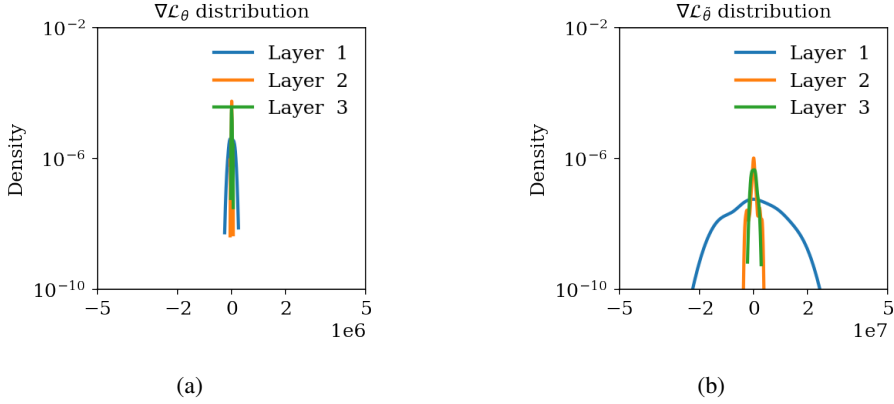


Figure 5: Impact of a differential operator in amplification of noise for the calculation of back propagated gradients: (a) distribution of the gradients of the parameters of our neural network model after training for 1000 epochs, (b) distribution of the gradients of the parameters of our neural network model at the perturbed state.

where $\|\cdot\|$ is a vector norm and G' is the derivative of G with respect to x . We use Eq. (8) to demonstrate ill-conditioning of solutions to PDEs that may become challenging to learn with neural networks.

2 Proposed Method: Preconditioned Physics and Equality Constrained Artificial Neural Networks

Consider the following second-order PDE

$$-\operatorname{div}(A \nabla u) + Xu = f, \quad \text{in } \Omega \in \mathbf{R}^d, \quad (9)$$

subject to the following boundary conditions

$$u = g_D, \text{ on } \Gamma_D, \text{ and } -\mathbf{n} \cdot A \nabla u = g_N, \text{ on } \Gamma_N, \quad (10)$$

where Ω is the domain with its boundary $\partial\Omega = \Gamma_D \cup \Gamma_N$ with $\Gamma_D \cap \Gamma_N = \emptyset$. $A(x)$ is a $d \times d$ symmetric matrix-valued function, X is a differential operator of order at most one, and \mathbf{n} is the outward normal unit vector to the boundary. f , g_D and g_N are source functions in Ω , Γ_D and Γ_N , respectively.

The problem defined by Eqs. (9) and (10) is generally non-symmetric and does not have any underlying minimization principle. Following the work of Cai et al. [33], we introduce a flux parameter σ , the problem defined by (9) and (10) can be written as a first-order system of PDE as follows:

$$\mathcal{D} = -\operatorname{div}(\sigma) + Xu - f \quad (11)$$

subject to the the following constraints

$$\mathcal{F} = \sigma - A \nabla u, \quad \text{in } \Omega, \quad (12)$$

$$\mathcal{B} = u - g_D, \quad \text{on } \Gamma_D, \quad (13)$$

$$\mathcal{N} = \mathbf{n} \cdot \sigma + g_N, \quad \text{on } \Gamma_N. \quad (14)$$

By introducing the flux variable σ , we reduced the second-order PDE in Eq. (9) to the first-order PDE in Eq. (11), which can then be used to learn by a single neural network model under the constraints presented in Eqs. (12)-(14). Consider the following constrained optimization problem

$$\min_{\theta} \sum_{i=1}^{N_D} \|\mathcal{D}(x^{(i)}; \theta)\|_2^2 \quad (15)$$

subject to the following constraints

$$-\epsilon \leq \mathcal{B}(x^{(i)}; \theta) \leq \epsilon, \quad \forall i = 1, \dots, N_{\mathcal{B}}, \quad (16)$$

$$-\epsilon \leq \mathcal{N}(x^{(i)}; \theta) \leq \epsilon, \quad \forall i = 1, \dots, N_{\mathcal{N}}, \quad (17)$$

$$-\epsilon \leq \mathcal{F}(x^{(i)}; \theta) \leq \epsilon, \quad \forall i = 1, \dots, N_{\mathcal{F}}, \quad (18)$$

where $\epsilon > 0$ is a small positive number. Our goal in the above constrained optimization is to minimize an objective function such that constraints are satisfied within a small range of errors $(-\epsilon, \epsilon)$. Without loss of generality, we can simplify our constraints as follows

$$\phi(\mathcal{B}(x^{(i)}; \theta)) \leq \epsilon, \quad \forall i = 1, \dots, N_{\mathcal{B}}, \quad (19)$$

$$\phi(\mathcal{N}(x^{(i)}; \theta)) \leq \epsilon, \quad \forall i = 1, \dots, N_{\mathcal{N}}, \quad (20)$$

$$\phi(\mathcal{F}(x^{(i)}; \theta)) \leq \epsilon, \quad \forall i = 1, \dots, N_{\mathcal{F}}, \quad (21)$$

where $\phi \in [0, \infty)$ is a convex distance function (i.e. absolute value function or quadratic function). Since the minimum of our distance function occurs at the minimum of its inputs, the above formulations for our constraints are equivalent. Therefore, by pushing the $\epsilon \rightarrow 0$, we get equality constraints as follows

$$\phi(\mathcal{B}(x^{(i)}; \theta)) = 0, \quad \forall i = 1, \dots, N_{\mathcal{B}}, \quad (22)$$

$$\phi(\mathcal{N}(x^{(i)}; \theta)) = 0, \quad \forall i = 1, \dots, N_{\mathcal{N}}, \quad (23)$$

$$\phi(\mathcal{F}(x^{(i)}; \theta)) = 0, \quad \forall i = 1, \dots, N_{\mathcal{F}}, \quad (24)$$

Next, we pursue the PECANN framework [28] to formulate an objective functional for the first-order system of PDEs. Given a set of $N_{\mathcal{D}}$ residual points $\{x^{(i)}\}_{i=1}^{N_{\mathcal{D}}}$ in the domain Ω , $N_{\mathcal{F}}$ residual points $\{x^{(i)}\}_{i=1}^{N_{\mathcal{F}}}$ in the domain Ω , $N_{\mathcal{B}}$ boundary points $\{(x^{(i)}, g_D^{(i)})\}_{i=1}^{N_{\mathcal{B}}}$ in Γ_D and $N_{\mathcal{N}}$ boundary points $\{(x^{(i)}, g_N^{(i)})\}_{i=1}^{N_{\mathcal{N}}}$ in Γ_N , we can write the following objective function

$$\mathcal{L}_{\mu}(\theta; \lambda) = \mathcal{L}_{\mathcal{D}}(\theta) + \mathcal{L}_{\mathcal{F}}(\theta; \lambda_{\mathcal{F}}) + \mathcal{L}_{\mathcal{B}}(\theta; \lambda_{\mathcal{B}}) + \mathcal{L}_{\mathcal{N}}(\theta; \lambda_{\mathcal{N}}) + \frac{\mu}{2} \pi(\theta), \quad (25)$$

where

$$\mathcal{L}_{\mathcal{D}}(\theta) = \sum_{i=1}^{N_{\mathcal{D}}} \|\mathcal{D}(x^{(i)}; \theta)\|_2^2, \quad (26)$$

$$\mathcal{L}_{\mathcal{F}}(\theta; \lambda_{\mathcal{F}}) = \sum_{i=1}^{N_{\mathcal{F}}} \lambda_{\mathcal{F}}^{(i)} \phi(\mathcal{F}(x^{(i)}; \theta)), \quad (27)$$

$$\mathcal{L}_{\mathcal{B}}(\theta; \lambda_{\mathcal{B}}) = \sum_{i=1}^{N_{\mathcal{B}}} \lambda_{\mathcal{B}}^{(i)} \phi(\mathcal{B}(x^{(i)}; \theta)), \quad (28)$$

$$\mathcal{L}_{\mathcal{N}}(\theta; \lambda_{\mathcal{N}}) = \sum_{i=1}^{N_{\mathcal{N}}} \lambda_{\mathcal{N}}^{(i)} \phi(\mathcal{N}(x^{(i)}; \theta)), \quad (29)$$

and the penalty term is as follows

$$\pi(\theta) = \pi_{\mathcal{F}}(\theta) + \pi_{\mathcal{B}}(\theta) + \pi_{\mathcal{N}}(\theta), \quad (30)$$

$$\pi_{\mathcal{F}}(\theta) = \sum_{i=1}^{N_{\mathcal{F}}} \|\phi(\mathcal{F}(x^{(i)}; \theta))\|^2, \quad (31)$$

$$\pi_{\mathcal{B}}(\theta) = \sum_{i=1}^{N_{\mathcal{B}}} \|\phi(\mathcal{B}(x^{(i)}; \theta))\|^2, \quad (32)$$

$$\pi_{\mathcal{N}}(\theta) = \sum_{i=1}^{N_{\mathcal{N}}} \|\phi(\mathcal{N}(x^{(i)}; \theta))\|^2, \quad (33)$$

where μ is a positive penalty parameter, $\lambda_{\mathcal{F}}$, $\lambda_{\mathcal{D}}$ and $\lambda_{\mathcal{N}}$ are vectors of Lagrange multipliers to enforce Eqs. (12), (13) and (14), respectively. These multipliers are responsible for adjusting the global learning rate based on their

corresponding loss functions. These vectors of Lagrange multipliers may also be viewed as preconditioning matrices that are diagonal with their elements set to the corresponding vectors of Lagrange multipliers. ϕ is a convex distance function. Using the update rule for the augmented Lagrangian method, we update the Lagrange multipliers as follows

$$\lambda_{\mathcal{F}}^{(i)} \leftarrow \lambda_{\mathcal{F}}^{(i)} + \mu\phi(\mathcal{F}(x^{(i)}; \theta)), \forall i = 1, \dots, N_{\mathcal{F}}, \quad (34)$$

$$\lambda_{\mathcal{B}}^{(i)} \leftarrow \lambda_{\mathcal{B}}^{(i)} + \mu\phi(\mathcal{B}(x^{(i)}; \theta)), \forall i = 1, \dots, N_{\mathcal{B}}, \quad (35)$$

$$\lambda_{\mathcal{N}}^{(i)} \leftarrow \lambda_{\mathcal{N}}^{(i)} + \mu\phi(\mathcal{N}(x^{(i)}; \theta)), \forall i = 1, \dots, N_{\mathcal{N}}, \quad (36)$$

where \leftarrow indicates an optimization step. Our training algorithm is the same as the one we presented in [28]. Next, we will discuss our choice for the distance function ϕ and its significance in learning the parameters of a physics-constrained neural network.

2.1 Role of Convex Distance Function in Training

Incorporation of a distance function ϕ in the learning algorithm is a novel idea that we introduced in our previous work [28]. In mathematical optimization, ϕ is an identity function [32, 37]. However, due to random initialization of neural network models, the identity distance function for measuring errors may result in cancellation of errors caused by either over- or under-prediction of the target function because total errors are accumulated over a set of training points. Therefore, an elegant way to get around this issue is to introduce a convex distance function $\phi \in [0, \infty)$ that has a minimum where errors are zero. Distance functions have the advantage of providing continuous feedback on the violation of constraints. We will use two cases to demonstrate the impact of distance functions. Let $\mathcal{L}_1(\theta; \lambda)$ be the loss function denoting the errors made on a Dirichlet type boundary conditions. Let's assume the prediction of our neural network model is \hat{u} and the exact boundary value is u . We can write the following objective function with an identity distance function as follows:

$$\mathcal{L}_1(\theta; \lambda) = \lambda(\hat{u} - u), \quad (37)$$

$$\frac{\partial \mathcal{L}_1}{\partial \theta} = \lambda \frac{\partial \hat{u}}{\partial \theta} \quad (38)$$

From Eq. (38) we observe that the back-propagated gradient does not include the information on the error (i.e., $\hat{u}_\theta - u$) induced by the model at the current optimization step.

Now let us consider the same case above with a quadratic distance function, which is convex, without loss of generality.

$$\mathcal{L}_2(\theta; \lambda) = \lambda(\hat{u} - u)^2, \quad (39)$$

$$\frac{\partial \mathcal{L}_2}{\partial \theta} = 2\lambda(\hat{u} - u) \frac{\partial \hat{u}}{\partial \theta} \quad (40)$$

We observe from Eq. (40) that the current error ($\hat{u}_\theta - u$) made on the boundary condition is informative, meaning that it appears on the right hand side of Eq. (40). This seemingly minor change significantly improves the convergence and robustness of the method as we have shown in our previous work [28].

2.2 Performance Metrics

We adopt the following metrics for evaluating the prediction of our models. Given an n -dimensional vector of predictions $\hat{\mathbf{u}} \in \mathbf{R}^n$ and an n -dimensional vector of exact values $\mathbf{u} \in \mathbf{R}^n$, we define a relative Euclidian or L^2 norm

$$\epsilon_r(\hat{\mathbf{u}}, \mathbf{u}) = \frac{\|\hat{\mathbf{u}} - \mathbf{u}\|_2}{\|\mathbf{u}\|_2}, \quad (41)$$

where $\|\cdot\|_2$ denotes the Euclidean norm. We also define a maximum norm

$$\epsilon_\infty(\hat{\mathbf{u}}, \mathbf{u}) = \|\hat{\mathbf{u}} - \mathbf{u}\|_\infty, \quad (42)$$

where $\|\cdot\|_\infty$ denotes the maximum norm.

3 Numerical Experiments

We apply our proposed method to learn the solution of several second-order PDEs that are prevalent in computational physics. We also compare our results with other published results to highlight the marked improvements in accuracy levels due to our proposed method.

3.1 Poisson's Equation

We consider a pedagogical elliptic PDE to demonstrate the application of our method and highlight its marked improvement over existing neural network-based methods. Learning an elliptic PDE can become challenging for neural network-based approaches that do not adequately constrain the boundary conditions [28, 27]. Here, we solve a one-dimensional Poisson's equation that is also considered in Cai et al. [33] to highlight our method. Consider the following differential equation

$$-\frac{d^2u(x)}{dx^2} = f(x), \quad x \in \Omega = (0, 1), \quad (43)$$

$$u(x) = 0, \quad x \in \partial\Omega = \{0, 1\} \quad (44)$$

where $f(x)$ is the source function. We manufacture a solution for Eq. (43) and its boundary conditions Eq. (44) as follows:

$$u(x) = x(e^{-(x-\frac{1}{3})^2/0.01} - e^{-\frac{4}{9}/0.01}) \quad (45)$$

The corresponding source functions $f(x)$ can be calculated exactly using Eq. (45). Unlike the approach in [33], we use a single neural network architecture that predicts the parameter of interest u and the flux variable $\sigma = -u_x(x)$. We note that the single neural network is enabled by the PECANN framework. A schematic representation of a multi-layer fully-connected feed-forward neural network architecture with ψ activation functions for a one-dimensional Poisson equation is given in Fig. 6.

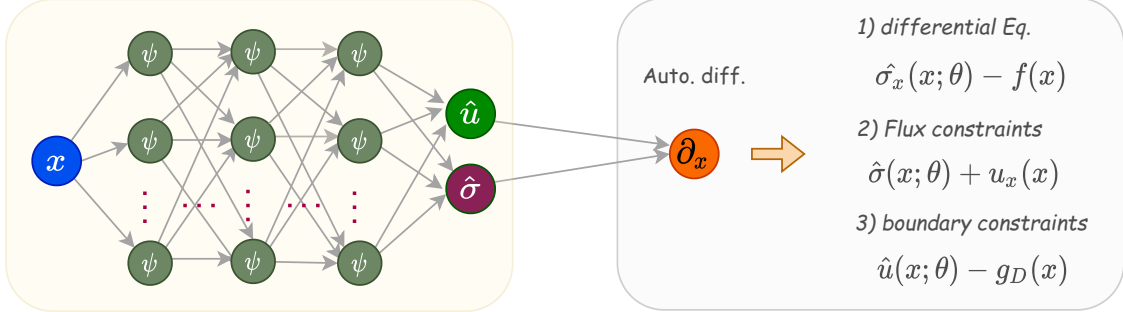


Figure 6: Schematic representation of our neural network architecture for a one-dimensional Poisson equation with ψ activation functions

We use a fully connected neural network architecture, which consists of one hidden layer with 24 neurons. We note that our network corresponds to the first layer of the composite neural network architecture in [33]. We sample $N_\Omega = 200$ residual points from the interior part of the domain only for once. We use the L-BFGS optimizer [38] with its default parameters and *strong Wolfe* line search function that is built in PyTorch framework [39]. We train our network for 20000 epochs with our safeguarding penalty parameter $\mu_{\max} = 10^4$ and a quadratic distance function $\phi(r) = r^2$.

We present the prediction of our neural network in Fig. 7(a). From Fig. 7(b), we observe that our neural network model has successfully learned the underlying solution. Next, we present the predicted flux obtained from our neural network model in Fig. 8(a). From Fig. 8(b), we observe that our neural network model has successfully learned the underlying flux.

Finally, we demonstrate the distribution of Lagrange multipliers for enforcing the flux equation $\sigma = -u_x(x)$ in Fig. 9. From Fig. 9 we observe that our model adaptively enforced regions of higher gradients by learning a vector of Lagrange multipliers to ensure the feasibility of flux constraints. Next, we present a summary of the medians of error norms over three independent trials with Xavier initialization scheme [40] in Table 1. The results reported in Table 1 show that our method achieves three orders of magnitude lower error than the one obtained by [33] with just a single layer of their composite neural network architecture. This improvement is not just due to properly enforcing the boundary condition but also properly imposing the flux equation as can be seen from the error levels obtained.

3.2 Heat Transfer in Composite Materials

In this section, we study a PDE problem with a non-smooth solution. This is a typical heat transfer in a composite material where temperature and heat fluxes are matched across the interface [41, 42]. Consider a one-dimensional

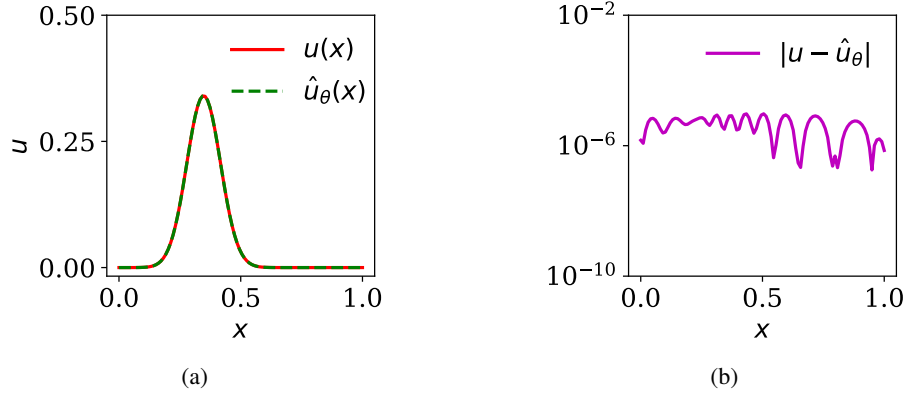


Figure 7: Poisson equation: (a) exact solution u vs the predicted solution \hat{u} with *sigmoid* activation function, (b) absolute point-wise error of the predicted solution

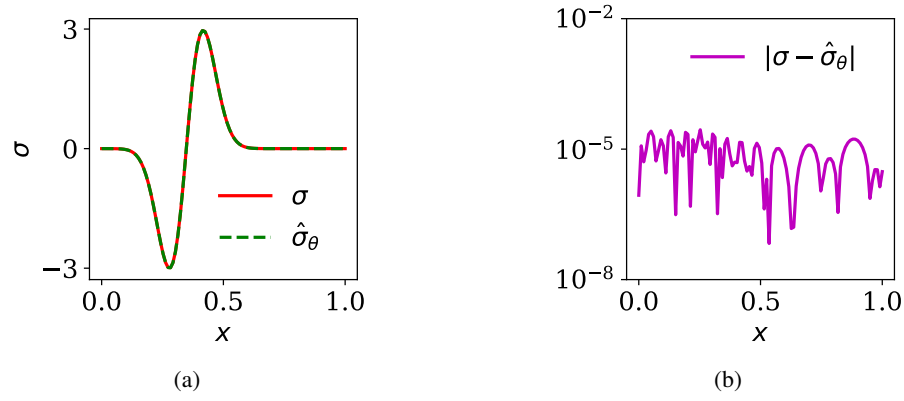


Figure 8: Poisson equation: (a) exact flux distribution σ and the predicted flux distribution $\hat{\sigma}$, (b) absolute point-wise error distribution of the predicted flux,(e) distribution of Lagrange multipliers for local flux constraints

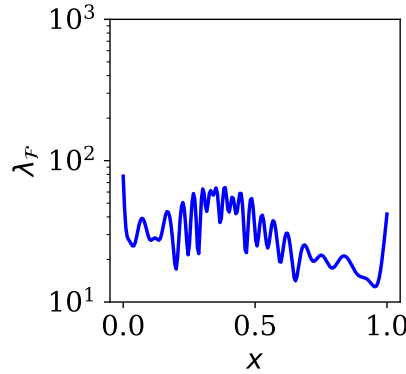


Figure 9: Distribution of Lagrange multipliers for local flux constraints for the Poisson's equation example.

interface equation, which is also considered in the work of Cai et al. [33],

$$-\frac{\partial}{\partial x} [a(x) \frac{\partial u(x)}{\partial x}] = f(x), \quad x \in \Omega = (0, 1), \quad (46)$$

$$u(x) = 0, \quad x \in \partial\Omega = \{0, 1\}, \quad (47)$$

Table 1: Summary of the median of error norms for the Poisson's equation example.

Models	$\epsilon_r(u, \hat{u})$	$\epsilon_r(\sigma, \hat{\sigma})$	N_Ω	No. Parameters
Ref. [33] (sigmoid)	1.351×10^{-2}	8.897×10^{-3}	200	1246
Current (sigmoid)	4.380×10^{-5}	1.308×10^{-5}	200	98

where $a = 1$ for $x \in (0, \frac{1}{2})$ and $a = k$ for $x \in (\frac{1}{2}, 1)$.

$$f(x) = \begin{cases} 8k(3x - 1), & x \in (0, \frac{1}{2}) \\ 2k(k + 1), & x \in (\frac{1}{2}, 1) \end{cases} \quad (48)$$

$$u(x) = \begin{cases} 4kx^2(1 - x), & x \in (0, \frac{1}{2}) \\ [2(k + 1)x - 1](1 - x), & x \in (\frac{1}{2}, 1). \end{cases} \quad (49)$$

Since the solution given in Eq. (49) is non-smooth, we cannot directly use Eq. (46). We can reduce Eq. (46) into a system of first-order differential equations by introducing an auxiliary flux parameter $\sigma = -au_x$. We use a fully connected neural network architecture, which consists of a one hidden layer with 32 neurons and sigmoid activation functions. Similar to [33], we sample $N_\Omega = 500$ residual points from the interior part of the domain only once. Our distance function in this problem is the Huber function [43] and we adopt the L-BFGS optimizer [38] with its default parameters and *strong Wolfe* line search function that are built in PyTorch framework [39]. We train our network for 20000 epochs with our safeguarding penalty parameter $\mu_{\max} = 1.0$.

We present the prediction of our neural network model in Fig. 10(a). From Fig. 10(b), we observe that our neural network model has successfully learned the underlying solution.

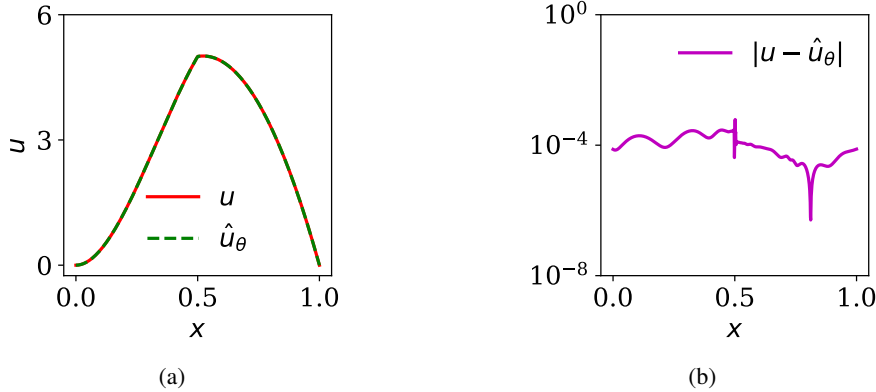


Figure 10: Interface problem: (a) exact solution vs. predicted solution, (b) absolute point-wise error of predicted solution.

Next, we present the predicted flux obtained from our neural network model in Fig. 11(a). From Fig. 11(b), we observe that our neural network model has successfully learned the underlying flux. Finally, we present the distribution of Lagrange multipliers for enforcing the flux constraints in Fig. 12.

From Fig. 12, we observe a spike in the distribution of Lagrange multipliers λ_F at the interface where fluxes are matched. This shows that our model has adaptively learned to focus on regions where the fluxes are challenging to learn to ensure the uniform feasibility of flux constraint across the domain.

We also present a summary of the medians of error norms over three independent trials with Xavier initialization scheme [40] in Table 2. The results indicate that our method achieves two orders of magnitude lower norms of error than the method presented in [33]. We also emphasize that in our approach we only use a single layer of the same neural network architecture used in Cai et al. [33], whereas Cai et al. use a composite architecture by design.

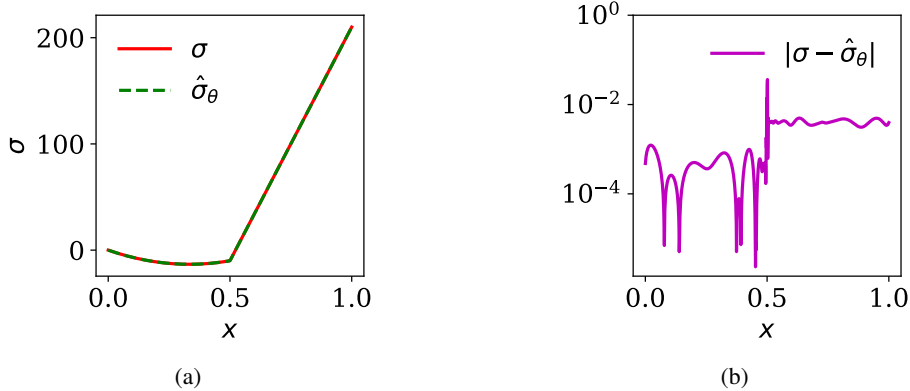


Figure 11: Interface problem: (c) exact flux distribution vs. predicted flux distribution, (d) absolute point-wise error distribution of predicted flux.

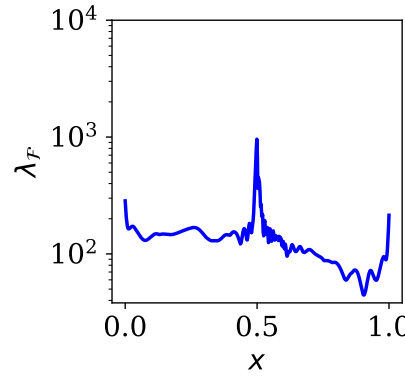


Figure 12: Interface problem: distribution of Lagrange multipliers for local flux constraints.

Table 2: Summary of the median of error norms for the interface problem.

Models	$\epsilon_r(u, \hat{u})$	$\epsilon_r(\sigma, \hat{\sigma})$	No. Parameters
Ref. [33] (sigmoid)	7.137×10^{-3}	1.870×10^{-3}	2962
Current (sigmoid)	4.654×10^{-5}	4.457×10^{-5}	130

3.3 Singularly Perturbed Reaction-Diffusion Equation

In this section, we study a singularly perturbed reaction-diffusion equation, which is also studied in [33].

$$-\epsilon^2 \frac{\partial^2 u(x)}{\partial x^2} + u(x) = f(x), \quad x \in \Omega = (-1, 1), \quad (50)$$

$$u(x) = 0, \quad x \in \partial\Omega = \{-1, 1\}, \quad (51)$$

where ϵ is the singular perturbation parameter. The manufactured solution presented in [33] is as follows

$$u(x) = \tanh\left(\frac{1}{\epsilon}(x^2 - \frac{1}{4})\right) - \tanh\left(\frac{3}{4\epsilon}\right), \quad (52)$$

with $\epsilon = 0.01$. Solutions to singularly perturbed problems with smooth data typically exhibit boundary layers whose width depends on the singular perturbation parameter. Therefore, learning them becomes challenging as ϵ becomes smaller. From Fig. 13(a), we observe that as ϵ decreases, the solution drastically changes which becomes challenging to capture with conventional numerical methods. From Figs. 14(a) and (b), we observe that for smaller values of ϵ ,

gradient of the solution becomes non-smooth, which becomes challenging to learn with the strong form the governing equation as in (51). To mathematically quantify this challenge, we derive a condition number for this problem in terms of ϵ .

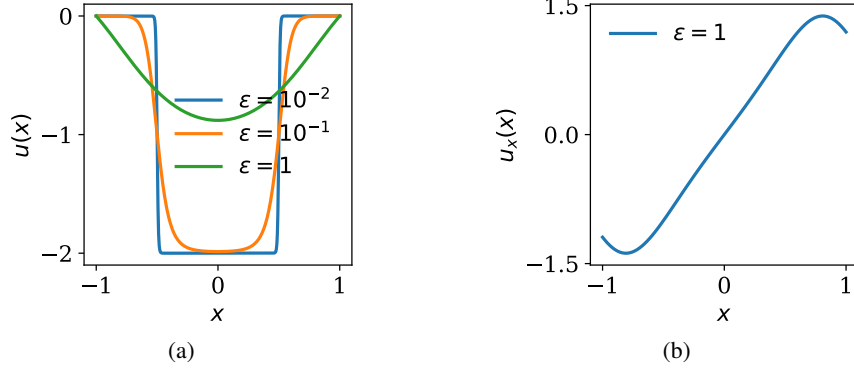


Figure 13: Singularity perturbed reaction diffusion equation: (a) exact solution for various ϵ , (b) exact gradient for $\epsilon = 1$.

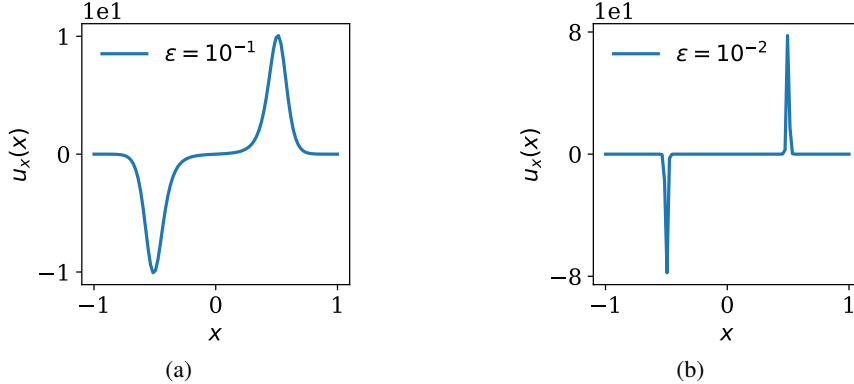


Figure 14: Singularity perturbed reaction diffusion equation: (c) exact gradient for $\epsilon = 10^{-1}$, (d) exact gradient for $\epsilon = 10^{-2}$.

To achieve this, we create a vector of inputs x with 100 elements and evaluate the solution $G(x)$ from Eq. (52) with its derivative $G'(x)$ exactly calculated. We then use Eq. (8) to approximate a condition number for decreasing values of ϵ . The resulting relative condition number $\kappa(x)$ is presented in Fig. 15. From Fig. 15, As ϵ decreases, the condition number of the problem increases, indicating that learning the solution becomes more complex.

Having discussed the complexity of learning the solution to this problem, we use neural networks to learn the solution for a challenging case when $\epsilon = 0.01$. For this purpose, we introduce a flux variable $\sigma = -\epsilon^2 u_x(x)$ as in [33]. We use a fully connected neural network architecture, which consists of three hidden layers with 32, 24, and 24 neurons respectively. We should note that our neural network architecture corresponds to a single branch of the composite neural network architecture presented in [33]. Our non-linearity activation function is sigmoid. Similar to [33], we sample $N_\Omega = 2000$ residual points from the interior part of the domain only once. Our optimizer is L-BFGS [38] with its default parameters and *strong Wolfe* line search function that is built in PyTorch framework [39]. We set our safeguarding penalty parameter $\mu_{\max} = 10^4$ and a quadratic distance function. We train our network for 10000 epochs with Adam optimizer. We initialize our learning rate to 10^{-2} and reduce it with a factor of 0.90 if no improvement the objective function is observed for a 100 epochs. After 10000 epochs, we switch to L-BFGS [38] optimizer with its default parameters and *strong Wolfe* line search function that is built in PyTorch framework [39]. We present the prediction of our neural network model in figure 16(a).

From figure 16(b), we observe that our neural network model has successfully learned the underlying solution. Next, we present the predicted flux obtained from our neural network model in Fig. 17(a). From Fig. 17(b), we observe that our model has successfully learned the underlying flux.

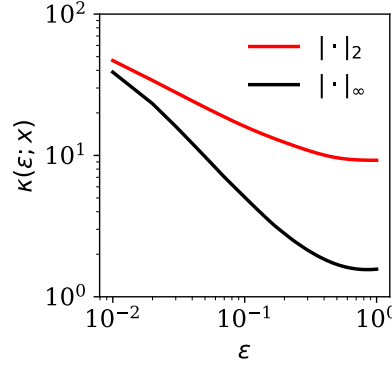


Figure 15: Singularly perturbed reaction diffusion equation: (a) relative condition number with L^2 and L^∞ norms versus ϵ

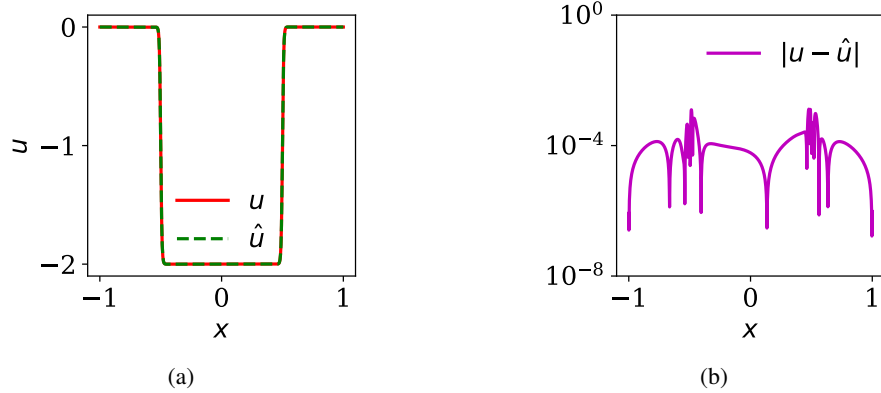


Figure 16: Singularly perturbed equation: (a) exact solution vs predicted solution, (b) absolute point-wise error of predicted solution

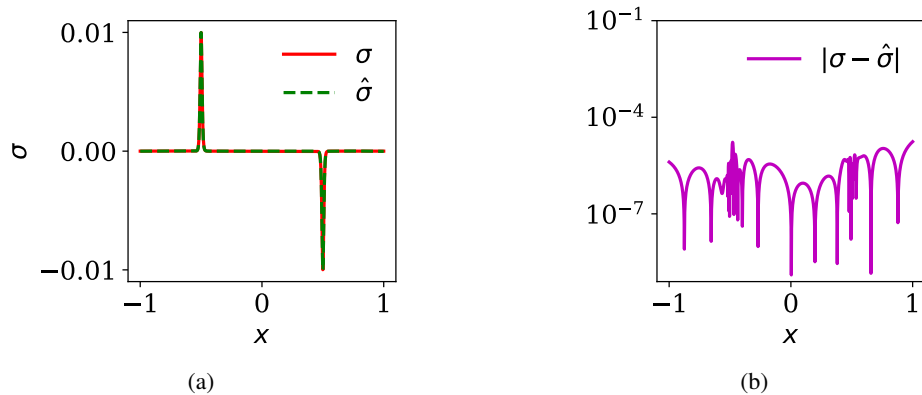


Figure 17: Singularly perturbed equation: (c) exact flux distribution vs. predicted flux distribution, (d) absolute point-wise error distribution of predicted flux

Finally, we present the distribution of Lagrange multipliers in Fig. 18, which peaks at two locations where there are drastic changes in flux and the solution. This shows that our model adaptively learned to focus on the regions where the solution becomes challenging to learn.

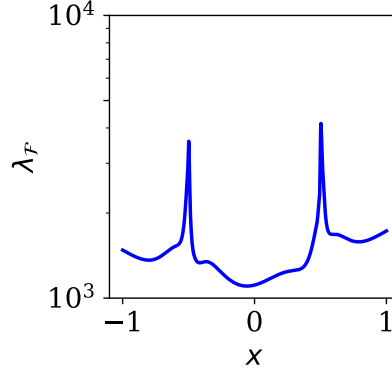


Figure 18: Singularly perturbed equation: (a) distribution of Lagrange multipliers for local flux constraints

In addition, we present the median of error norms over three independent trials with random Xavier initialization scheme[40] in Table 3. We observe that the relative error $\epsilon_r(\sigma, \hat{\sigma})$ obtained from our model is two orders of magnitude lower than the one obtained [33] with a single branch of their composite neural network model.

Table 3: Summary of the median of error norms for the singularly perturbed equation.

Models	$\epsilon_r(u, \hat{u})$	$\epsilon_r(\sigma, \hat{\sigma})$	No. Parameters
Ref. [33] (sigmoid)	1.403×10^{-3}	2.115×10^{-1}	2962
Current (sigmoid)	2.743×10^{-4}	3.830×10^{-3}	1506

3.4 Convection-dominated convection-diffusion equation

A wide range of physical problems involves diffusive and convective (transport) processes. Standard numerical methods work well when diffusion dominates convection. However, standard numerical methods such as finite differences or standard Galerkin finite elements become unstable when convection effects dominates over diffusion effects [44]. Consider the following problem that is also studied in the work of van der Meer et al. [23]

$$v \frac{du(x)}{dx} + \alpha \frac{d^2u(x)}{dx^2} = 0, \quad \text{in } \Omega, \quad (53)$$

$$u = g(x), \quad \text{on } \partial\Omega \quad (54)$$

where $v = 1$, α is the diffusivity coefficient, $\Omega = \{x \mid 0 \leq x \leq 1\}$ with its boundary $\partial\Omega$. The analytical solution of the above equation is given as follows

$$u(x) = \frac{e^{-\frac{vx}{\alpha}}}{1 - e^{-\frac{v}{\alpha}}} - \frac{1}{2}. \quad (55)$$

From Eq. (55), we observe that the size of the boundary layer is proportional to the diffusivity coefficient α . Therefore, the solution becomes challenging as α is decreased. Solution of convection-dominated convection-diffusion problems can result in boundary layers in which the solution behaves drastically differently in a small part of the domain. Therefore, learning a solution for these types of PDEs can become challenging. From Fig. 19, we observe that as α decreases, the solution drastically changes, which becomes challenging to capture with conventional numerical methods. This complexity can be seen from the sudden change in the flux distribution as demonstrated in Fig. 20.

To mathematically quantify this challenge, we derive a condition number for this problem in terms of ϵ . To achieve this, we create a vector of inputs x with 100 elements and evaluate the solution $G(x)$ from Eq. (55) with its derivative $G'(x)$ exactly calculated. We then use Eq. (8) to approximate a condition number for decreasing values of ϵ . The resulting condition number is presented in Fig. (21). From Fig. (21), we observe that as we decrease α , the condition number of the problem increases, which indicates the increasing complexity of learning the solution.

Having discussed the complexity of learning the solution of this problem, we use neural networks to learn the solution for a challenging case for which $\alpha = 10^{-4}$. We achieve this by introducing an auxiliary flux parameter $\sigma(x) = -\alpha \frac{du(x)}{dx}$

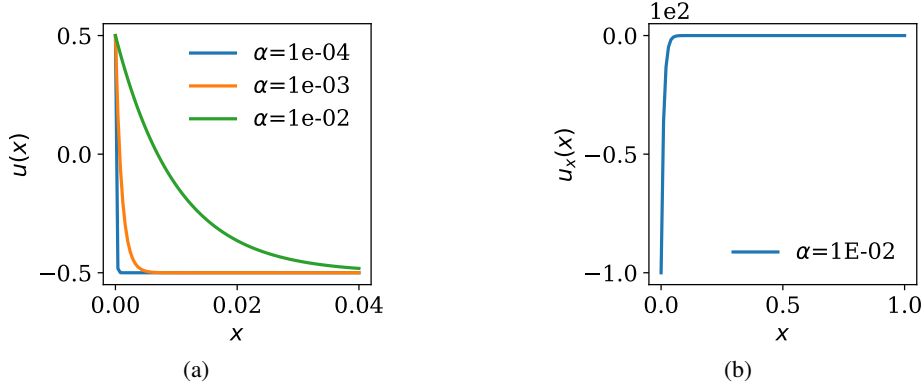


Figure 19: Convection dominated convection-diffusion equation: (a) exact solution for various α , (b) exact gradient for $\alpha = 10^{-2}$

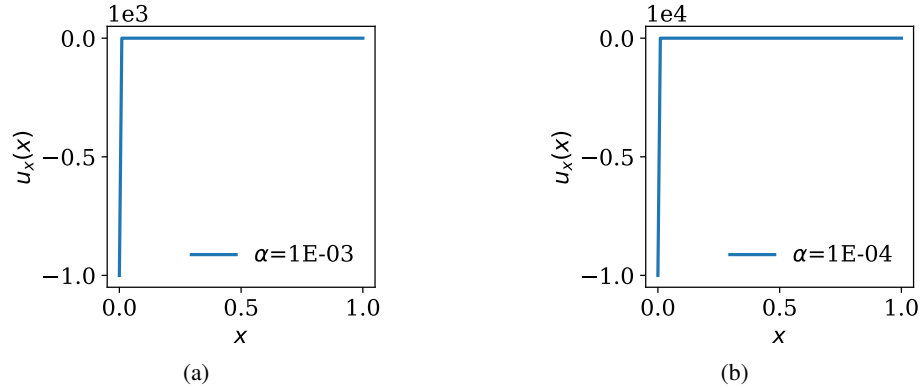


Figure 20: Convection dominated convection-diffusion equation: (a) exact gradient for $\alpha = 10^{-3}$, (b) exact gradient for $\alpha = 10^{-4}$

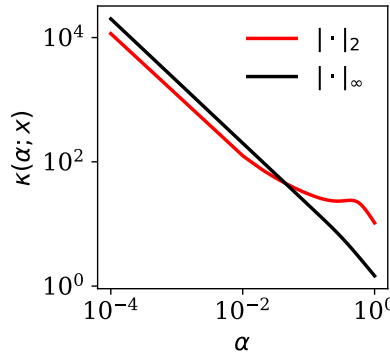


Figure 21: convection dominated convection diffusion equation: condition number with L^2 and L^∞ norms vs. α

to reduce Eq. (53) to a system of first-order partial differential equations. For this problem, we use a fully connected feed-forward neural network with one hidden layer and 20 neurons. We should note that our network corresponds to a single layer of the neural network architecture used in [23]. Our network employs tangent hyperbolic non-linearity and has one input and two outputs corresponding to u and σ . We adopt the L-BFGS optimizer with its default parameters that are built-in PyTorch framework [39] and we train our network for 2000 epochs. We use Huber [43] function as our distance function and set our safeguarding penalty parameter $\mu_{\max} = 10^4$.

We present the prediction of our neural network model in Fig. 22(a). From Fig. 22(b), we observe that our model has accurately learned the underlying solution. Next, We present the prediction of our neural network model in Fig. 23(a). From Fig. 23(b), we observe that our model has accurately learned the underlying flux.

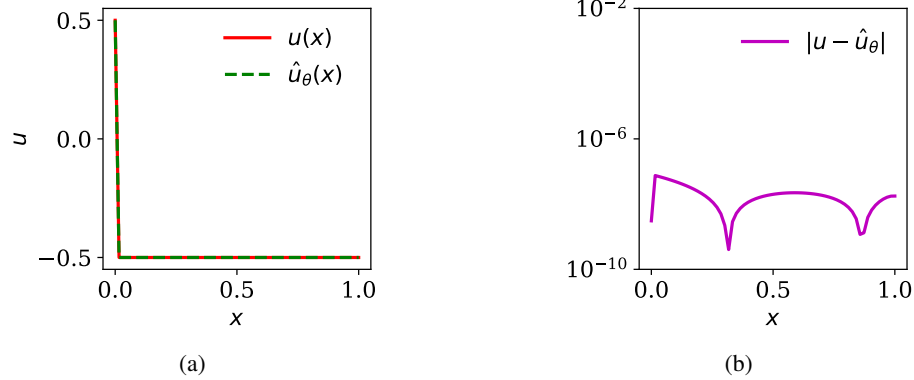


Figure 22: Convection-dominated convection diffusion equation: (a) exact solution u vs the predicted solution \hat{u} , (b) absolute point-wise error of the predicted solution

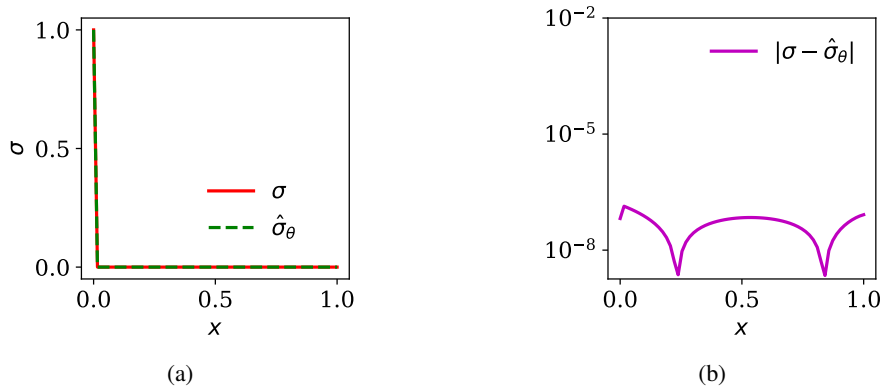


Figure 23: Convection-dominated convection diffusion equation: (a)exact flux distribution σ and the predicted flux distribution $\hat{\sigma}$, (d) absolute point-wise error distribution of the predicted flux

Finally, we present the distribution of Lagrange multiplier in Fig. 24, which shows that our model has learned to focus on the regions that are challenging to learn.

In addition, in Table 4 we present the error norms obtained from different methods with random Xavier initialization scheme [40]. We observe that the relative error $\epsilon_r(u, \hat{u})$ obtained from our model is eighth orders of magnitude lower than the one obtained in [23]. We are also able to achieve this level of high accuracy with a single layer of their neural network architecture trained for one-tenth of the number of epochs used in [23].

Table 4: Convection-diffusion: summary of error norms obtained from different methods

Method	α	$\epsilon_r(u, \hat{u})$	$\epsilon_\infty(u, \hat{u})$	Sampling Strategy	No.Parameters	Epochs
Optimal Loss Weight[23]	10^{-4}	1.15×10^0	2.00×10^0	Adaptive	1341	20×10^3
Magnitude Normalization.[23]	10^{-4}	1.91×10^0	3.51×10^1	Adaptive	1341	20×10^3
Proposed method	10^{-4}	5.19×10^{-8}	7.52×10^{-8}	Uniform	82	2×10^3

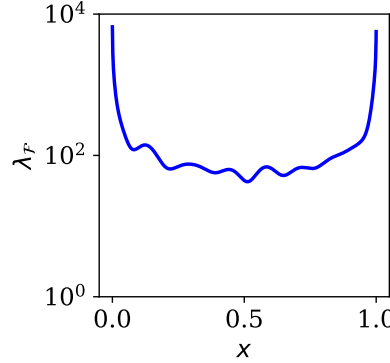


Figure 24: Convection-dominated convection diffusion equation: distribution of Lagrange multipliers for local flux constraints

4 Conclusion

High-order differential operators are sources for amplification of learning complexity in physics informed/constrained neural networks. We have demonstrated this issue by injecting perturbations in the outputs obtained from a neural network model during training, which have produced high levels of noise in a structured loss function that is composed of differential operators. Consequently, back-propagated gradients are corrupted by the high-level of noise impeding the convergence of the learning process. We have also quantified this learning complexity issue by computing the relative condition number of a solution.

To mitigate these challenges associated with learning the solution of second-order PDEs, we preconditioned the differential operators by introducing an auxiliary flux variable as proposed in [33] and obtained a system of first-order PDEs. We then formulated a constrained optimization problem to minimize the residual on the reduced-order PDE subject to its boundary conditions and the auxiliary flux equation. Constraining the flux equation not only provide an adaptive mechanism that enforces regions of higher gradients but also allows for information exchange between the flux variable and primary variable. We extended our PECANN framework [28] and demonstrated that a single neural-network architecture, as opposed to a composite architecture with two branches, is sufficient to learn the solution arising from a system of first-order PDEs. This simplicity in the architecture is possible because the PECANN framework enables re-usability and sharing of learned features by the flux variable and the primary variable in a single network. We applied our methodology to various challenging second-order PDE problems and demonstrated orders of magnitude improvements over other published results that adopt different approaches with neural networks.

5 Acknowledgments

This material is based upon work supported by the National Science Foundation under Grant No. 1953204 and in part in part by the University of Pittsburgh Center for Research Computing through the resources provided.

References

- [1] K. Hornik, M. Stinchcombe, H. White, Multilayer feedforward networks are universal approximators, *Neural Netw.* 2 (1989) 359–366.
- [2] M. W. M. G. Dissanayake, N. Phan-Thien, Neural-network-based approximations for solving partial differential equations, *Commun. Numer. Meth. Eng.* 10 (1994) 195–201.
- [3] B. P. van Milligen, V. Tribaldos, J. A. Jiménez, Neural network differential equation and plasma equilibrium solver, *Phys. Rev. Lett.* 75 (1995) 3594–3597.
- [4] C. Monterola, C. Saloma, Solving the nonlinear schrodinger equation with an unsupervised neural network, *Opt. Express* 9 (2001) 72–84.
- [5] M. Quito Jr, C. Monterola, C. Saloma, Solving N-body problems with neural networks, *Physical review letters* 86 (2001) 4741.
- [6] D. Parisi, M. C. Mariani, M. Laborde, Solving differential equations with unsupervised neural networks, *Chem. Eng. Process.* 42 (2003) 715–721.

[7] M. Hayati, B. Karami, Feedforward neural network for solving partial differential equations, *J. Appl. Sci.* 7 (2007) 2812–2817.

[8] I. E. Lagaris, A. Likas, D. I. Fotiadis, Artificial neural networks for solving ordinary and partial differential equations, *IEEE Trans. Neural Netw.* 9 (1998) 987–1000.

[9] W. E, B. Yu, The deep Ritz method: A deep learning-based numerical algorithm for solving variational problems, *Commun. Math. Stat.* 6 (2018) 1–12. doi:doi:10.1007/s40304-018-0127-z.

[10] M. Raissi, P. Perdikaris, G. Karniadakis, Physics-informed neural networks: A deep learning framework for solving forward and inverse problems involving nonlinear partial differential equations, *J. Comput. Phys.* 378 (2019) 686–707.

[11] J. Sirignano, K. Spiliopoulos, DGM: A deep learning algorithm for solving partial differential equations, *J. Comput. Phys.* 375 (2018) 1339–1364.

[12] M. Abadi, P. Barham, J. Chen, Z. Chen, A. Davis, J. Dean, M. Devin, S. Ghemawat, G. Irving, M. Isard, M. Kudlur, J. Levenberg, R. Monga, S. Moore, D. G. Murray, B. Steiner, P. Tucker, V. Vasudevan, P. Warden, M. Wicke, Y. Yu, X. Zheng, TensorFlow: A system for large-scale machine learning, in: *Proceedings of the 12th USENIX Conference on Operating Systems Design and Implementation*, OSDI’16, USENIX Association, USA, 2016, p. 265–283.

[13] M. Raissi, Z. Wang, M. S. Triantafyllou, G. E. Karniadakis, Deep learning of vortex-induced vibrations, *J. Fluid Mech.* 861 (2019) 119–137.

[14] G. Kissas, Y. Yang, E. Hwang, W. R. Witschey, J. A. Detre, P. Perdikaris, Machine learning in cardiovascular flows modeling: Predicting arterial blood pressure from non-invasive 4D flow MRI data using physics-informed neural networks, *Comput. Method. Appl. Mech. Eng.* 358 (2020) 112623.

[15] Z. Mao, A. D. Jagtap, G. E. Karniadakis, Physics-informed neural networks for high-speed flows, *Computer Methods in Applied Mechanics and Engineering* 360 (2020) 112789.

[16] A. D. Jagtap, E. Kharazmi, G. E. Karniadakis, Conservative physics-informed neural networks on discrete domains for conservation laws: Applications to forward and inverse problems, *Computer Methods in Applied Mechanics and Engineering* 365 (2020) 113028.

[17] M. Aliakbari, M. Mahmoudi, P. Vadasz, A. Arzani, Predicting high-fidelity multiphysics data from low-fidelity fluid flow and transport solvers using physics-informed neural networks, *International Journal of Heat and Fluid Flow* 96 (2022) 109002. URL: <https://www.sciencedirect.com/science/article/pii/S0142727X22000777>. doi:doi:<https://doi.org/10.1016/j.ijheatfluidflow.2022.109002>.

[18] R. G. Patel, I. Manickam, N. A. Trask, M. A. Wood, M. Lee, I. Tomas, E. C. Cyr, Thermodynamically consistent physics-informed neural networks for hyperbolic systems, *Journal of Computational Physics* 449 (2022) 110754. URL: <https://www.sciencedirect.com/science/article/pii/S0021999121006495>. doi:doi:<https://doi.org/10.1016/j.jcp.2021.110754>.

[19] S. Amini Niaki, E. Haghigheh, T. Campbell, A. Poursartip, R. Vaziri, Physics-informed neural network for modelling the thermochemical curing process of composite-tool systems during manufacture, *Computer Methods in Applied Mechanics and Engineering* 384 (2021) 113959. URL: <https://www.sciencedirect.com/science/article/pii/S0045782521002966>. doi:doi:<https://doi.org/10.1016/j.cma.2021.113959>.

[20] Y. Chen, L. Lu, G. E. Karniadakis, L. D. Negro, Physics-informed neural networks for inverse problems in nano-optics and metamaterials, *Opt. Express* 28 (2020) 11618–11633. URL: <http://opg.optica.org/oe/abstract.cfm?URI=oe-28-8-11618>. doi:doi:10.1364/OE.384875.

[21] M. M. Almajid, M. O. Abu-Al-Saud, Prediction of porous media fluid flow using physics informed neural networks, *Journal of Petroleum Science and Engineering* 208 (2022) 109205. URL: <https://www.sciencedirect.com/science/article/pii/S0920410521008597>. doi:doi:<https://doi.org/10.1016/j.petrol.2021.109205>.

[22] H. Gao, L. Sun, J.-X. Wang, Phygeonet: Physics-informed geometry-adaptive convolutional neural networks for solving parameterized steady-state pdes on irregular domain, *Journal of Computational Physics* 428 (2021) 110079. URL: <https://www.sciencedirect.com/science/article/pii/S0021999120308536>. doi:doi:<https://doi.org/10.1016/j.jcp.2020.110079>.

[23] R. van der Meer, C. W. Oosterlee, A. Borovykh, Optimally weighted loss functions for solving PDEs with neural networks, *CoRR* abs/2002.06269 (2020).

[24] L. McClenny, U. Braga-Neto, Self-adaptive physics-informed neural networks using a soft attention mechanism, *arXiv preprint arXiv:2009.04544* (2020).

[25] S. Wang, Y. Teng, P. Perdikaris, Understanding and mitigating gradient flow pathologies in physics-informed neural networks, *SIAM Journal on Scientific Computing* 43 (2021) A3055–A3081.

[26] A. Krishnapriyan, A. Gholami, S. Zhe, R. Kirby, M. W. Mahoney, Characterizing possible failure modes in physics-informed neural networks, *Advances in Neural Information Processing Systems* 34 (2021).

[27] S. Basir, I. Senocak, Critical Investigation of Failure Modes in Physics-informed Neural Networks, 2021. URL: <https://arc.aiaa.org/doi/abs/10.2514/6.2022-2353>. doi:doi:10.2514/6.2022-2353. arXiv:<https://arc.aiaa.org/doi/pdf/10.2514/6.2022-2353>.

[28] S. Basir, I. Senocak, Physics and equality constrained artificial neural networks: Application to forward and inverse problems with multi-fidelity data fusion, *J. Comput. Phys.* (2022) 111301. URL: <https://www.sciencedirect.com/science/article/pii/S0021999122003631>. doi:doi:<https://doi.org/10.1016/j.jcp.2022.111301>.

[29] R. Bischof, M. Kraus, Multi-objective loss balancing for physics-informed deep learning, *arXiv preprint arXiv:2110.09813* (2021).

[30] F. S. Lobato, V. Steffen Jr, Multi-objective optimization problems: concepts and self-adaptive parameters with mathematical and engineering applications, Springer, 2017.

[31] M. J. Powell, A method for nonlinear constraints in minimization problems, in: R. Fletcher (Ed.), Optimization; Symposium of the Institute of Mathematics and Its Applications, University of Keele, England, 1968, Academic Press, London, New York, 1969, pp. 283–298.

[32] D. P. Bertsekas, Multiplier methods: A survey, *Automatica* 12 (1976) 133–145.

[33] Z. Cai, J. Chen, M. Liu, X. Liu, Deep least-squares methods: An unsupervised learning-based numerical method for solving elliptic pdes, *Journal of Computational Physics* 420 (2020) 109707.

[34] A. G. Baydin, B. A. Pearlmutter, A. A. Radul, J. M. Siskind, Automatic differentiation in machine learning: a survey, *Journal of Machine Learning Research* 18 (2018) 1–43.

[35] H. Li, Z. Xu, G. Taylor, C. Studer, T. Goldstein, Visualizing the loss landscape of neural nets, *Advances in neural information processing systems* 31 (2018).

[36] A. Quarteroni, R. Sacco, F. Saleri, Numerical mathematics, volume 37, Springer Science & Business Media, 2010.

[37] M. R. Hestenes, Multiplier and gradient methods, *J. Optim. Theory Appl.* 4 (1969) 303–320.

[38] J. Nocedal, Updating quasi-Newton matrices with limited storage, *Math. Comput.* 35 (1980) 773–782.

[39] A. Paszke, S. Gross, F. Massa, A. Lerer, J. Bradbury, G. Chanan, T. Killeen, Z. Lin, N. Gimelshein, L. Antiga, et al., Pytorch: An imperative style, high-performance deep learning library, *Advances in neural information processing systems* 32 (2019).

[40] X. Glorot, Y. Bengio, Understanding the difficulty of training deep feedforward neural networks, in: Y. W. Teh, M. Titterington (Eds.), *Proceedings of the Thirteenth International Conference on Artificial Intelligence and Statistics*, volume 9 of *Proceedings of Machine Learning Research*, PMLR, Chia Laguna Resort, Sardinia, Italy, 2010, pp. 249–256.

[41] A. Lahiri, 5 - transport phenomena and metals properties, in: S. Seetharaman (Ed.), *Fundamentals of Metallurgy*, Woodhead Publishing Series in Metals and Surface Engineering, Woodhead Publishing, 2005, pp. 178–236. URL: <https://www.sciencedirect.com/science/article/pii/B9781855739277500054>. doi:doi:<https://doi.org/10.1533/9781845690946.1.178>.

[42] J. Baker-Jarvis, R. Inguva, Heat conduction in layered, composite materials, *Journal of applied physics* 57 (1985) 1569–1573.

[43] P. J. Huber, Robust estimation of a location parameter, in: *Breakthroughs in statistics*, Springer, 1992, pp. 492–518.

[44] J. M. Fiard, T. A. Manteuffel, S. F. McCormick, First-order system least squares (fosls) for convection-diffusion problems: Numerical results, *SIAM Journal on Scientific Computing* 19 (1998) 1958–1979.